Improved Harmonic Mitigation Using Dual Three-Phase iUPQC

Y Anil Kumar[1*], *P. Swathi*[2], *Vajjala Venkata, Anjali Prasanna*[3], *G. Veera Sankara Reddy*[4] and Sareddy Venkata Rami Reddy[5]

[1]Department of Electrical and Electronics Engineering, Vignana Bharathi Institute of Technology, Hyderabad, India.
[2]Department of Electrical and Electronics Engineering, JNTUACEA Anantapur-515002, India
[3]Department of Electrical Engineering, IIIT RGUKT, RK VALLEY, Idupulapaya, Vempalli -516330, India
[4]Department of Electrical and Electronics Engineering, JNTUA College of Engineering Pulivendula, Pulivendula-516390, India.
[5]Department of Electrical and Electronics Engineering, JNTUA College of Engineering Pulivendula, Pulivendula-516390, India.

Abstract. This study simplifies iUPQC administration by employing a dual three-phase design, which makes the methodology behind the study more transparent. By utilising a parallel (shunt) and series active filter, it is possible to limit the amount of harmonics and unbalances produced by the iUPQC. When compared to a conventional UPQC, an iUPQC modifies the series filter in such a way that it operates as a sinusoidal current source. This is in contrast to a conventional UPQC. Since the iUPQC is regulated using voltage and current sinusoidal references rather than non-sinusoidal references, the frequency spectrum of the pulse width modulation (PWM) controls is well-known. This is because the iUPQC uses sinusoidal references rather than non-sinusoidal references. The study of power flow, as well as simulation and design control, are included in this paper.

1 Introduction

Power supply dependability and quality are becoming more critical. Voltage sags, swells, harmonics, and power disturbances may damage sensitive electronic equipment and hamper electrical system efficiency. The Dual Unified Power Quality Conditioner (DUPQC) is one of several power conditioning devices designed to improve power quality. The advanced Dual Unified Power Quality Conditioner corrects voltage and current abnormalities to enhance power quality. A series converter and a shunt converter provide significant power conditioning [1].

This article proposes a simplified control mechanism for the Dual Unified Power Quality Conditioner. The control method produces reliable power conditioning with reduced complexity and computational overhead. VSI and PI controllers govern series and shunt converters in the simplified control technique. Decoupled control lets series and shunt converters fix voltage and current abnormalities.

* Corresponding author: yaramala84@gmail.com

The streamlined control system correctly assesses power quality issues using sophisticated data processing techniques including voltage sag/swell detection, harmonic identification, and reactive power compensation. These computations provide converters with power quality-correcting control signals. Simplified control enhances dynamic responsiveness, computational complexity, and reliability. By simplifying the control algorithm without sacrificing performance, the Dual Unified Power Quality Conditioner is more practical and cheaper for wide industrial and commercial use. As transient loads' energy consumption has skyrocketed, the distribution system network has used more power quality conditioners [2]. Nonlinear loads' high harmonic content distorts utility grid voltage, affecting essential loads. A unified power quality conditioner (UPQC) may drain undistorted utility grid currents and provide loads with regulated, balanced, low-harmonic distortion voltage. UPQC active filters are parallel and series. SAFs balance grid voltage, whereas PAFs correct load harmonic current as non-sinusoidal current sources. Both have a harmonic control reference, frequently produced using complicated methods. Multiple-research suggest shunt and SAFs use sinusoidal reference control without harmonic extraction to facilitate the UPQC's reference development. Line voltage regulator/conditioners might replace power quality conditioners. This conditioner's two single-phase current source inverters control SAF and PAF with separate voltage and current loops. Sinusoidal grid current, load voltage, and references [1] [2].

N.G. Hingrani [3] is credited with introducing the notion of power. Diodes, thyristors, IGBTs, and diodes all make up power electronics devices [4]. Active power filters are used to completely sinusoidalize the supply current and remove harmonics from the load side current. Additionally, they make load side voltages balanced and of a comparable magnitude and aid in reducing supply voltage imbalance problems, such as voltage rise/dip. The active power filters may be incorporated to eliminate problems brought on by harmonics in both voltage and current. There are several techniques to regulate active power filters [5]. The [6] Three-phase, three-wire lines were modelled using reactive power theory since it is applicable in both dynamic and static situations. The instantaneous reactive power hypothesis' physical consequences were analysed in [7]. In [8 – 15] different controller and UPQC employed voltage source inverters also called as "dual configuration of unified power quality conditioner" (iUPQC) are discussed. P-q theory requires real-time voltage and current positive sequence component calculations for control approaches. A utility grid-connected dual three-phase integrated unified power quality conditioner (iUPQC) will be controlled efficiently by this study. ABC reference frame control uses traditional control scheme without coordinate conversions or digital control. Sinusoidal SAF and PAF references do not reduce grid current and load voltage harmonics.

2 Dual UPQC

Fig.1 shows the basic UPQC design with a SAF and PAF. The SAF operates as a voltage source to correct unbalances, grid distortion, and disturbances like swells, sags, and flashing. SAF-adjusted voltage contains fundamental and harmonic components. PAF current sources rectify load current imbalances, displacement, and harmonics to maintain a sinusoidal grid current. In low-voltage grid applications, the shunt filter connects directly to the load, whereas the series filter links to the utility grid via a transformer. In standard UPQC, series connection transformer leakage inductance influences voltage compensation by the series filter, and compound harmonic abstraction of the grid voltage and load requires elaborate derivative analysis.

This work examines the iUPQC (Fig. 2) to mitigate these shortcomings. The iUPQC uses the SAF and PAF together like the classic UPQC, but it regulates the filters in series and shunt. SAF, a current source in the iUPQC, enforces a sinusoidal input current phase-locked

to the grid voltage. The PAF becomes a sinusoidal load voltage source when plugged into the electrical grid. The iUPQC controller describes both active filters as sinusoids.

Sinusoidal reference production requires just that it be in phase with the utility's voltage supply, hence this is important for the conventional design. Due to the equal and opposite voltages across the connecting transformers from the grid voltage and load voltage, the SAF works as a high impedance for current harmonics, indirectly compensating for grid voltage harmonics, unbalances, and disturbances. The harmonic load current may help smooth out supply imbalances, shifting, and other distortions, similar to the PAF's low-impedance conduit for grid current harmonics.

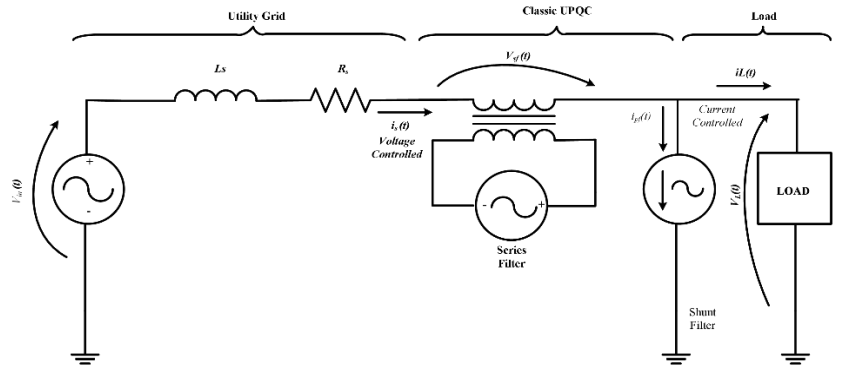

Fig. 1. Traditional UPQC structure.

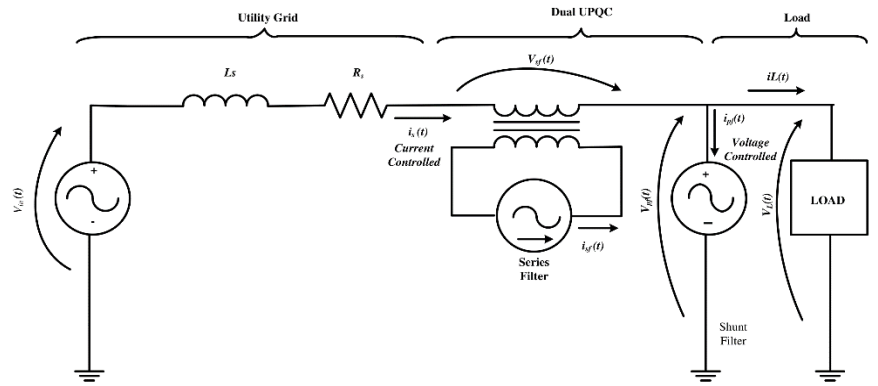

Fig. 2 Structure of Dual UPQC (iUPQC).

3 The passive output design of filter

A one-phase schematic helps explain the iUPQC circuit. vsc and vpc are voltage sources Similar series and shunt filter topologies create a fundamental component and harmonics from switch commutation, where $Zs = j\omega Ls + Rs$ represents the utility grid impedance and $Zlg = j\omega Llg + Rlg$, represents the coupling transformer leakage impedance. The iUPQC's output passive filters must eliminate high-frequency disturbances to preserve sinusoidal load voltages and grid currents. SAF and PAF output impedance investigation needs two equivalent circuits. Treating the series-connected voltage source vsc and inductance Lsf as a single current source simplified PAF analysis. The similar circuits show that the PAF's output impedance modifies the SAF's frequency response while having no

influence on it. Thus, the PAF design should precede the SAF design in the iUPQC output passive filter design.

$$\frac{v_L(s)}{v_{pc}(s)} = \frac{1}{L_{pf}C_{pf}} \cdot \frac{1}{s^2 + s \cdot \frac{1}{C_{pf}R_L} + \frac{1}{L_{pf}C_{pf}}} \quad (1)$$

The filter's cut-off frequency will decide the capacitor Cpf because the power design selected the inductor Lpf. The cut-off frequency of 2.9 kHz requires a 10F Cpf filter capacitor. PAF frequency response with and without load. By examining the circuit, the SAF's high-frequency filter transfer function may be calculated.

$$\frac{i_s(s)}{V_{sc}(s)} = \frac{n}{\{sL_{sf} + n^2[sL_{lg} + R_{lg} + \alpha + \beta].\gamma\}} \quad (2)$$

Where

$$\alpha = \frac{sL_{pf}R_L}{s^2L_{pf}C_{pf}R_L + sL_{sf} + R_L} \quad (3)$$

$$\beta = \frac{sL_{rd} + R_{rd}}{s^2L_sC_{sf} + sC_{sf}R_s + 1} \quad (4)$$

$$\gamma = s^2C_{sf}L_s + sC_{sf}R_{lg} + 1 \quad (5)$$

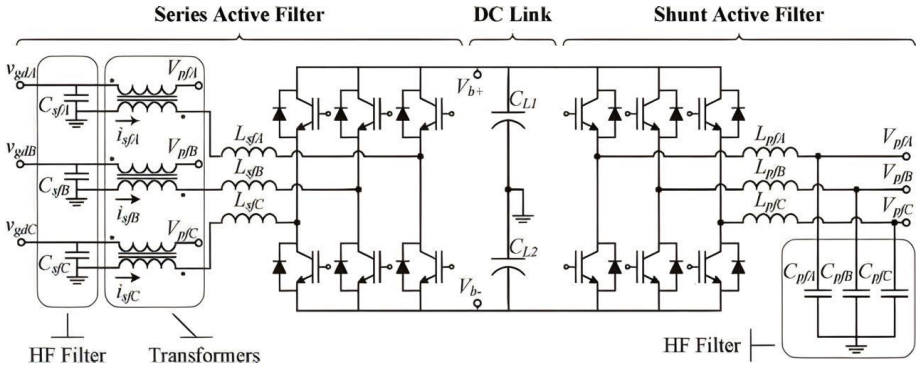

Fig. 3. The iUPQC's electrical power supply.

The filter's cut-off frequency will decide the capacitor Csf because the power design determined the inductor Lsf. The Csf was 1F at 45 Hz. Normal and no-load SAF frequency response. The filter response's low cut-off frequency decreases the SAF's bandwidth, reducing its effectiveness with harmonic quantity in the grid voltage. This low-frequency minimization is intrinsic to the coupling transformers' leakage impedance and extremely undesirable.

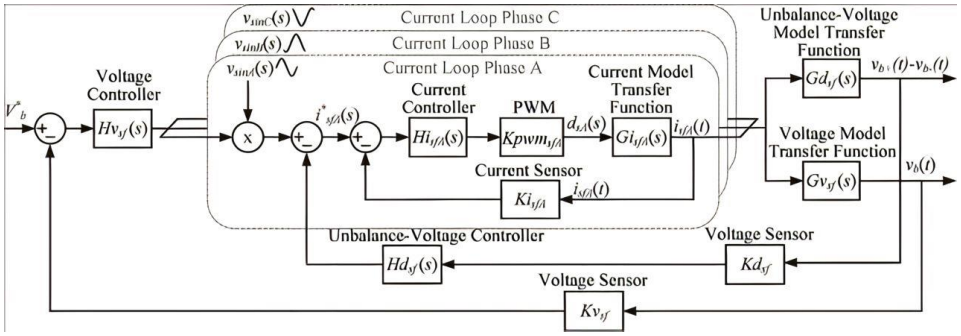

Fig. 4. SAF Controller schematic diagram.

4 Equations and mathematics

The ABC-based iUPQC control architecture suggests decoupled SAF and PAF control. Since the control approach compensates for harmonics, unbalances, disturbances, and displacement, power calculations and harmonic extraction are unnecessary. A current loop in the SAF keeps grid current sinusoidal and in phase with grid voltage. PAF's voltage loop reduces harmonic distortion and preserves load voltage. Each active filter has its own feedback loops. The SAF can manage dc connection voltage like power factor converters, where the current loop utilises the voltage loop as a reference for its amplitude.

4.1 Handling of the SAF

Fig. 4 shows SAF block diagram authority. SAF controls three identical dual voltage and current loops. Current loops must track each grid input phase to individually manage grid currents. In a dc link architecture, two voltage loops manage voltage and avoid capacitor imbalances. The entire dc voltage control loop slows input voltage variations and sets the current loop reference amplitude. As the load increases, the dc link voltage drops, exceeding the input grid current. This voltage regulator raises grid current reference to re-establish dc link voltage. As demand declines, the voltage controller reduces grid current reference to adjust dc link voltage. Rb represents the peak current across the dc connection at a particular moment and is not in the circuit. Since the utility grid voltage frequency results in zero instantaneous, the dc connection converts passive to active power consumption quickly. Calculate the usual dc link charging current as,

$$\overline{I_{eq}} = \frac{3}{2}.\frac{n.V_{gdpk}.I_{sfpk}}{V_b} \tag{6}$$

SAF current max No distinction is needed since the three phases have the same I_{sfpk}. Step (6) defines the Voltage Loop Transfer Function quantitatively.

$$G_{vsf}(s) = \frac{V_b(s)}{I_{sf}(s)} = \frac{3}{2}.n.\frac{V_{gdpk}}{V_b}.\frac{1}{\frac{1}{R_b} + sC_b} \tag{7}$$

where
V_{gdpk} maximum voltage on the grid;
Vb low voltage dc link;
Rb same resistance under a load;
Cb equivalent capacitance of all dc links;
transformation ratio n.
"Open-loop transfer function" ($OLTFv$) is given by

$$OLTF_v(s) = Gv_{sf}(s).\frac{Kv_{sf}}{Ki_{sf}}.Km_{sf} \tag{8}$$

where
$Kmfs$ multiplier gain;
$Kvsf$ voltage sensor amplitude;
$Kisf$ sensor gain at the moment.
The $Kmfs$ gain is derived by comparing the DSP's synchronised sinusoidal signal peak to the multiplier integrated circuit's gain. The integral of a percentage (PI)+pole controller controls voltage across the dc connection while ensuring a 4Hz crossover and 45degree phase difference. The voltage's frequency response is the sum of the open loop, controller, and compensated loop transfer functions ($OLTFv + Hvsf$). A low-frequency loop based on the grid current reference's dc level regulates imbalanced voltage in dc link capacitors.

This loop balances CL1 and CL2 by adding a dc level to the grid current references upon voltage mismatch detection. By replacing the switches of the inverter with two current sources, the four-wire converter permits single-phase analysis. D(t) is the duty cycle; neutral point current is isc(t). Laplace and meshing derive the unbalanced-voltage loop transfer function.

$$G_{dsf}(s) = \frac{V_b + (s) - V_b - (s)}{I_{sc}(s)} = \frac{3}{2.s.C_b} \quad (9)$$

The open-loop transfer function ($OLTFd$) is written by

$$OLTF_d(s) = Gd_{sf}(s).\frac{Kd_{sf}}{Ki_{sf}} \quad (10)$$

Where,

$Kdsf$ gain of differential voltage sensor. To reduce the differential dc link voltage, a PI with pole regulator was created to ensure 50 degrees of phase difference at 0.5 hertz. The voltage loop differential frequency response includes functional transfer in an open loop ($OLTFd$), regulator transfer function ($Hdsf$), and compensated loop transfer function ($OLTFd + Hdsf$). These situations stabilize the voltages vs(t) and vL(t). Laplace small-signal analysis provides the loop current transfer function.

$$G_{ifs}(s) = \frac{I_{sc}(s)}{D(s)} = \frac{V_b}{sA_1 + n^2.(R_s + R_{lg})} \quad (11)$$

Where

$$A_1 = n^2.(L_s + L_{lg}) + L_{sf} \quad (12)$$

The inductance of the grid in series (Ls),
The resistance of the grid (Rs),
Series inductance (Ls),
Resistance (Rs),
Leakage inductance (Llg) of the coupling transformer.
The coupling transformer has a series resistance of Rlg.
Function of the open loop transfer ($OLTFi$) is given by

$$OLTFi(s) = Gi_{sf}(s) \cdot Kpwm_{sf}.Ki_{sf} \quad (13)$$

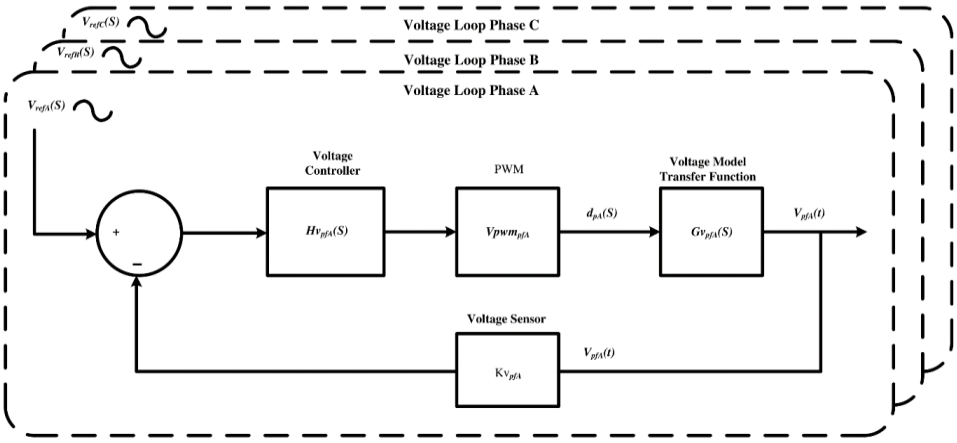

Fig. 5. Open loop controller of the SAF.

Where,

$Kpwmsf$ Modulator gain for a series filter using PWM (pulse width modulation). $Kpwmsf$ The triangle carrier's peak value serves as the inverse of the gain's formula. A PI+ pole

controller was developed with the intention of following the existing reference; this controller guarantees a crossover frequency of 5 kHz and a phase margin of 70. $OLTFi$, $Hisf$, and $OLTFi + Hisf$, which represent the open-loop, controller, and compensated loop transfer functions, respectively, are presented in Fig. 5, which depicts the frequency response of the current loop.

4.2 Handling of the SAF

The PAF control system consists of three identical load voltage feedback loops, separated by 120 phase shifts from their respective references. Laplace and small-signal analysis may be used to determine the voltage loop's transfer function.

$$Gv_{pf}(s) = \frac{V_b}{L_{pf}C_{pf}} \cdot \frac{1}{s^2 + s\left(\frac{1}{C_{pf}R_L}\right) + \frac{1}{L_{pf}C_{pf}}} \quad (14)$$

where $Gvpf$ (s) = VL(s)/D(s).
The open-loop transfer function ($OLTFvpf$) is given by

$$OLTF_v(s) = Gv_{pf}(s).Kpwm_{pf}.Kv_{pf} \quad (15)$$

Where $Kpwmpf$ high-gain shunt filter PWM modulator. We designed a proportional integral derivative (PID) controller with an additional pole for voltage reference monitoring, ensuring a crossover frequency of 4 kHz and a phase margin of 35. $OLTFvpf, Hvpf$, a corrected loop transfer function, and the voltage loop's frequency responsiveness, transfer function ($OLTFvpf + Hvpf$).

5 Simulation Results

5.1 Case – 1

Fig. 6(a) illustrates the source side voltage, which is of three-phase in single axis, individual phases are identified as red, blue, and green. The waveform is shown in a period of 0.5 S and the magnitude is about 180 V. Fig. 6(b) describes the source side current, which is of three-phase in single axis, individual phases are identified based on their colour coding such as red, blue, and green. The waveform is shown in a period of 0.5 S and the magnitude of current which is altering between +15 V to -15 V.

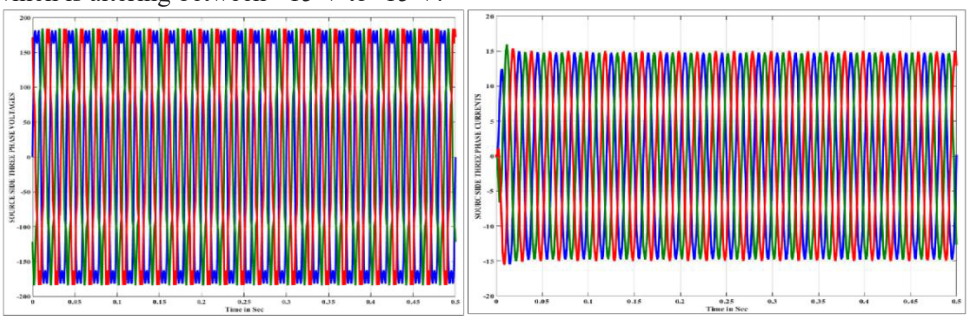

(a) (b)

Fig.6. (a) Three-phase Source Side Voltage, (b) Three-phase Source Side Current.

Fig. 7(a) demonstrates the source side voltage and current on a single axis that is of single phase only. Voltage is indicated by blue colour, and current is indicated by green in colour. Waveforms are shown in a period of 0.5 S and voltage magnitude is maintained about 90 V (upper and lower peaks) and current about 75 A. Fig. 7(b) shows the source side voltage and

current on a single axis that is of single phase only. Voltage is indicated by blue colour, and current is indicated by green in colour. Waveforms are shown in a period of 0.5 S and voltage magnitude is maintained at 90 V (upper and lower peaks) and current about 75 A. Fig. 7(c) shows the source side voltage and current on a single axis that is of single phase only. Voltage is indicated by blue colour, and current is indicated by green in colour. Waveforms are shown in a period of 0.5 S and voltage magnitude is maintained at 90 V (upper and lower peaks) and current about 75 A.

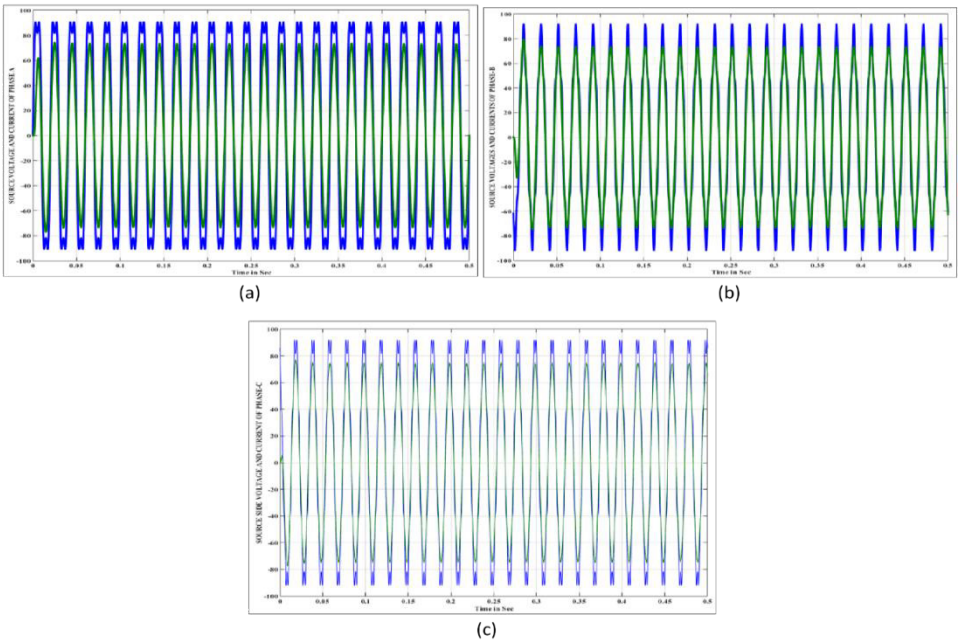

Fig. 7. (a) Source Voltage & Current waveforms of phase A, (b) Source Side Voltage & Current waveforms of phase B, (c) Source Side Voltage & Current waveforms of phase C

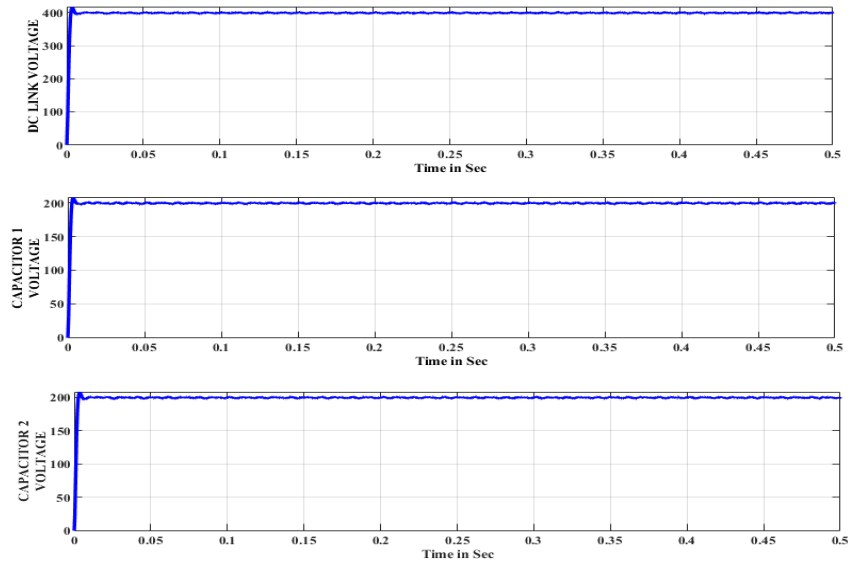

Fig. 8. a) DC link voltage, b & c) Capacitor voltages

Fig. 8(a) illustrates the dc link voltage which shows its dynamic and steady state responses at a period of 0.5 S and it reaches a magnitude of 400 V. Fig. 8(b) & (c) illustrates both the

capacitor dynamic & steady-state response voltages which has a magnitude of 200 V on y-axis. Fig. 9(a) demonstrates the voltages after passing through the series AP filter circuit. Each phase is different in terms of waveforms. All three waveforms are shown in a period of 0.5 S. Phase A voltage has a magnitude of 80 V. Phase B voltage has a magnitude of 48 V. Phase C voltage has a magnitude of 58 V. Fig. 9(b) demonstrates the currents after passing through the shunt AP filter circuit. Each phase is different in terms of waveforms. All three waveforms are shown in a period of 0.5 S. Phase A current has a magnitude of 10 A. Phase B current has a magnitude of 12 A. Phase C current has a magnitude of 16 A.

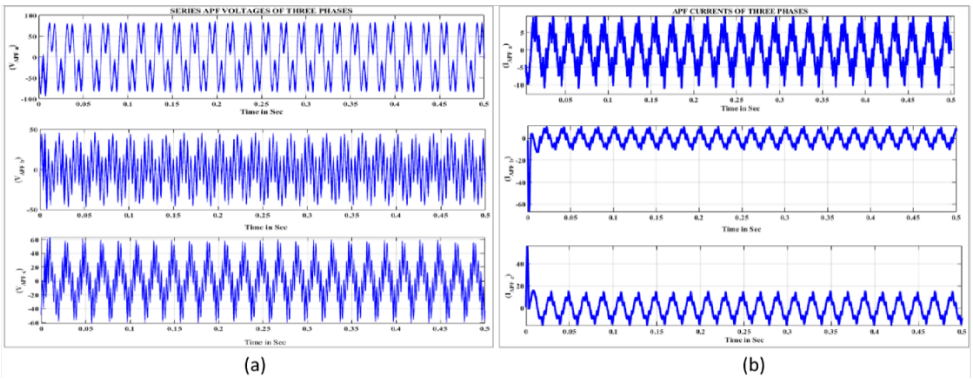

Fig. 9. (a) Three-phase series APF voltages, (b) Three-phase shunt APF voltages

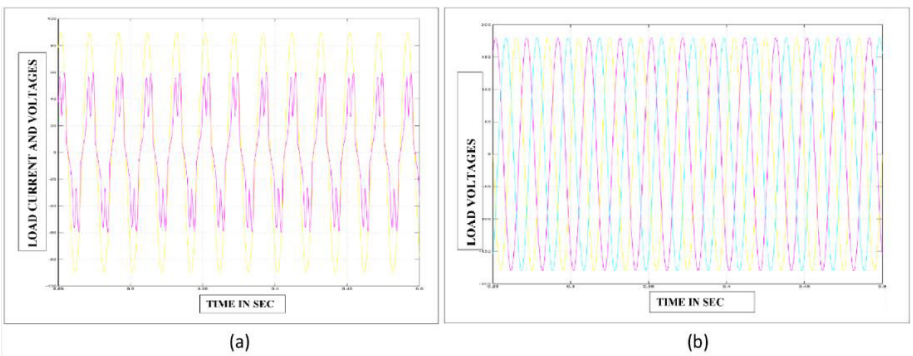

Fig. 10. (a) load side current and voltages of single-phase, (b) Load side voltages of Three-Phase

Fig. 10(a) demonstrates the currents and voltage at load side. Voltage magnitude is above 80 V and current magnitude is above 60 A. Pink colour waveform indicates the current wave form and yellow colour waveform indicates the voltage. Fig. 10(b) demonstrates the voltages at load side. Three phase Voltage magnitude is above 170 V. Three phases are indicated by different colouring such as yellow, pink and blue colour for each phase respectively.

5.2 Case – 2

Fig. 11(a) illustrates the source side voltage, which is of three-phase in single axis, individual phases are identified as red, blue, and green. The waveform is shown in a period of 0.5 S and the magnitude of voltage is about 180 V. Fig. 11(b) describes the source side current, which is of three-phase in single axis, individual phases are identified based on their colour coding such as red, blue, and green. The waveform is shown in a period of 0.5 S and the magnitude of current which is altering between +9 A to -9 A, and then increased to 12.5 A.

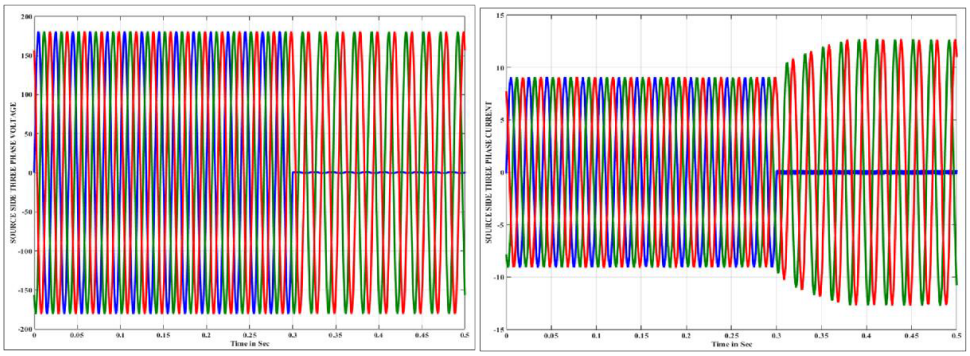

(a) (b)

Fig. 11. (a) Source Side Three-phase Voltage, (b) Source Side Three-phase Current

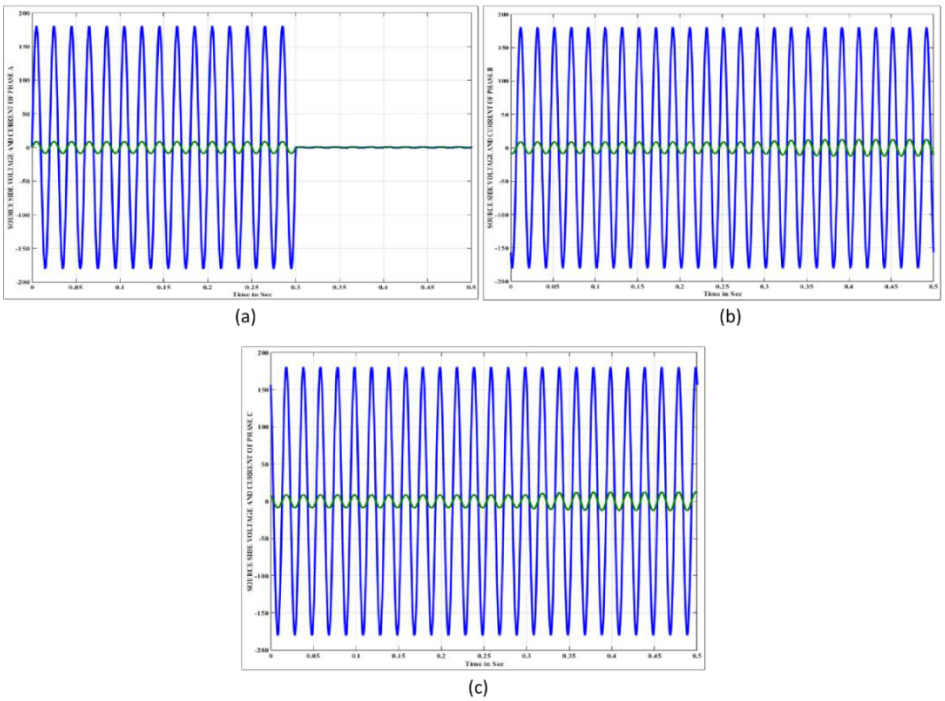

(a) (b)

(c)

Fig. 12. (a) Source Side Voltage & Current waveforms of phase A, (b) Source Side Voltage & Current waveforms of phase B, (c) Source Side Voltage & Current waveforms of phase C

Fig. 12(a) demonstrates the source side voltage and current on a single axis that is of single phase only. Voltage is indicated by blue colour, and current is indicated by green in colour. Waveforms are shown in a period of 0.5 S and voltage magnitude is maintained about 160 V (upper and lower peaks) and current about 10 A. Voltage and current becomes zero after 0.3 S. Fig. 12(b) shows the source side voltage and current on a single axis that is of single phase only. Voltage is indicated by blue colour, and current is indicated by green in colour. Waveforms are shown in a period of 0.5 S and voltage magnitude is maintained at 160 V (upper and lower peaks) and current about 10 A. Fig. 12(c) shows the source side voltage and current on a single axis that is of single phase only. Voltage is indicated by blue colour, and current is indicated by green in colour. Waveforms are shown in a period of 0.5 S and voltage magnitude is maintained at 160 V (upper and lower peaks) and current about 10 A.

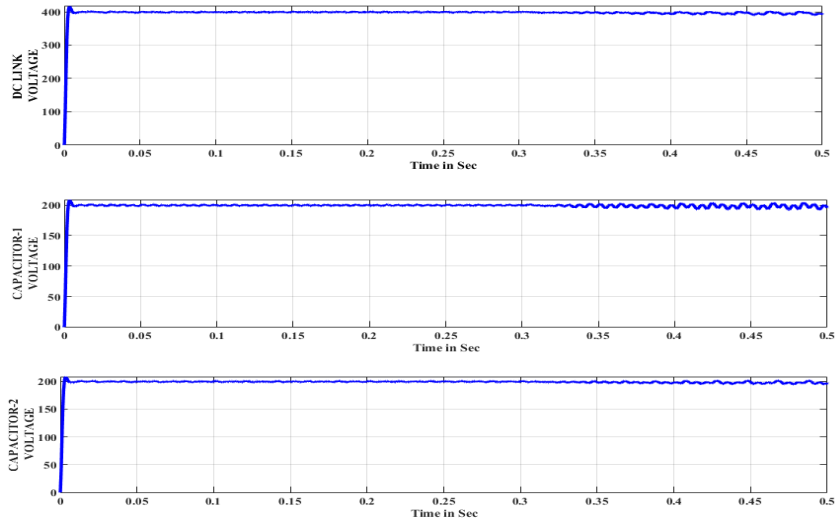

Fig. 13(a) dc link voltage, (b) & (c) capacitors voltages

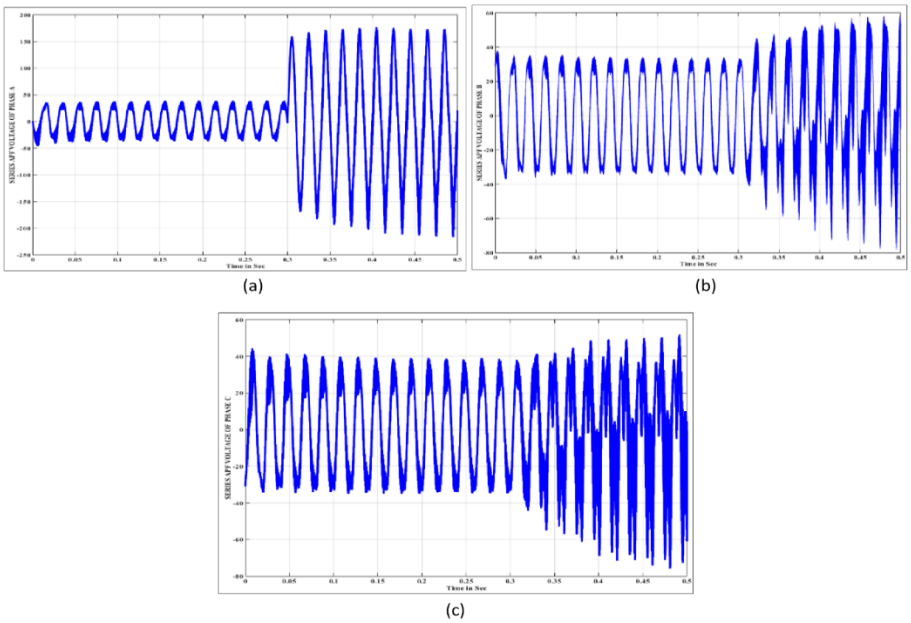

Fig. 14. (a) Series APF voltage of phase A, (b) Series APF voltage of phase B, (c) Series APF voltage of phase A

Fig. 13. (a) illustrates the dc link voltage which shows its dynamic as well as steady state responses at a period of 0.5 S and it reaches a magnitude of 400 V. Fig. 13(b) & (c) illustrates both the capacitor dynamic & steady-state response voltages which has a magnitude of 200 V on y-axis. Fig. 14(a) demonstrates the voltage after passing through the series AP filter circuit. Waveform is shown in a period of 0.5 S. Voltage magnitude is maintained at 40 V, up to 0.3 S and later it is raised to 160 V. Fig. 14(b) demonstrates the voltage after passing through the series AP filter circuit. Waveform is shown in a period of 0.5 S. Voltage magnitude is maintained at 30 V, up to 0.3 S and later it is raised to 80 V. Fig. 14(c) demonstrates the voltage after passing through the series AP filter circuit. Waveform is

shown in a period of 0.5 S. Voltage magnitude is maintained at 30 V, up to 0.3 S and later it is raised to 75 V.

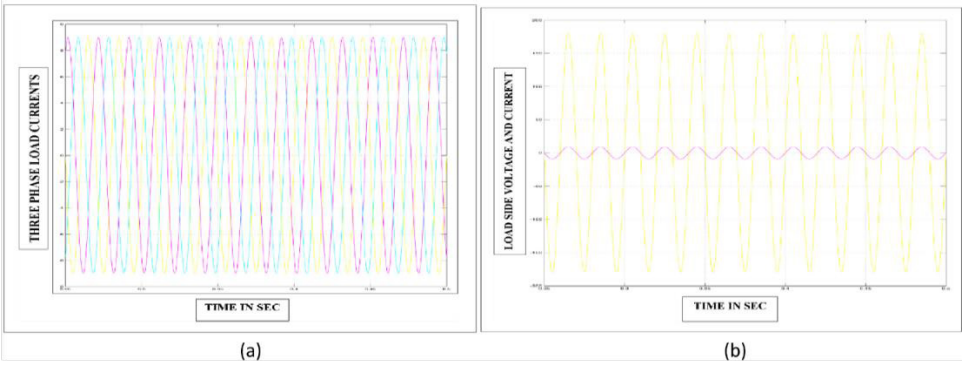

Fig. 15. (a) Three-phase load currents (b) single-phase load voltage and current

Fig. 15(a) demonstrates the currents at load side. Three phase current magnitude is altered between at +9 to -9 A. Three phases are indicated by different colouring such as yellow, pink and blue colour for each phase respectively. Fig. 15(b) demonstrates the currents and voltage at load side. Voltage magnitude is above 170 V and Current magnitude is above 10 A. Pink colour waveform indicates the current wave form and yellow colour waveform indicates the voltage.

6 CONCLUSION

The ABC reference frame control adjusted nonlinear load currents and assured sinusoidal voltage throughout all three phases, according to the iUPQC. Control performed well under power plant load stages and voltage disturbances. This control was superior than others because it used sinusoidal references for series and shunt active filter controls without complicated calculations or coordinate conversions, iUPQC references need grid voltage synchronisation, not harmonic content. The voltage of leakage impedance of the SAF connected transformer does not affect load voltage adjustment when utilising iUPQC in low-voltage distribution system networks since PAF directly controls load voltage. Distorted grid voltages result in leakage impedance that disrupts the current loop bandwidth, thereby reducing frequency responsiveness. These results support the iUPQC control system by showing that a simple control system may improve power quality.

References

1. K. Hasan, M. M. Othman, S. T. Meraj, S. Mekhilef, A. F. Bin Abidin, Shunt Active Power Filter Based on Savitzky-Golay Filter: Pragmatic Modelling and Performance Validation, in IEEE Transactions on Power Electronics, vol. 38, no. 7, pp. 8838-8850, 2023.
2. S. Devassy and B. Singh, Performance Analysis of Solar PV Array and Battery Integrated Unified Power Quality Conditioner for Microgrid Systems, in IEEE Transactions on Industrial Electronics, vol. 68, no. 5, pp. 4027-4035, May 2021.
3. N. Hingorani, Introducing Custom Power, in IEEE Spectrum, vol. 32, issue 6, pp. 41-48, June 1995.

4. C. D. Sanjenbam, B. Singh and P. Shah, Power Quality Enhancement of Stand-Alone Hydro Power Generation System Using UPQC, in IEEE Transactions on Industrial Informatics, vol. 20, no. 10, pp. 12062-12071, Oct. 2024.
5. Y.-W. Wang, M.-C. Wong, and C.-S. Lam, Historical Review of Parallel Hybrid Active Power Filter for Power Quality Improvement, in Proceedings of TENCON 2015 - IEEE Region 10 Conference, Macao, China, 2015, pp. 1-6.
6. S. S. Bhosale, Y. N. Bhosale, U. M. Chavan, and S. A. Malvekar, Power Quality Improvement by Using UPQC: A Review, in Proceedings of the 2018 International Conference on Control, Power, Communication and Computing Technologies (ICCPCCT), Kannur, India, 2018, pp. 375-380.
7. S. Singh and S. S. Letha, Various Custom Power Devices for Power Quality Improvement: A Review, in Proceedings of the 2018 International Conference on Power Energy, Environment and Intelligent Control (PEEIC), Greater Noida, India, 2018, pp. 689-695.
8. M. A. Chaudhari and Chandraprakash, Three-Phase Series Active Power Filter as Power Quality Conditioner, in Proceedings of the IEEE International Conference on Power Electronics, Drives and Energy Systems, Dec. 2012, pp. 1-6.
9. J. Smith and R. Lee, Advanced Unified Power Quality Conditioner for Modern Grid Applications, in IEEE Transactions on Power Electronics, vol. 38, no. 5, pp. 4521-4532, 2023.
10. P. Gonzalez and S. Ahmed, Enhancements in iUPQC for Power Quality Improvement in Distributed Systems, in Electric Power Systems Research, vol. 208, p. 107878, 2022.
11. V. Kumar and D. Patel, Performance Comparison of UPQC and iUPQC with Sinusoidal Control Techniques, in IEEE Transactions on Industrial Electronics, vol. 70, no. 4, pp. 2873-2885, 2023.
12. C. Fernandez and T. Silva, Dual Control Strategies for iUPQC to Enhance Harmonic Compensation, in IET Power Electronics, vol. 15, no. 8, pp. 1214-1224, 2022.
13. K. Rao and L. Huang, Hybrid Compensation Strategies in UPQC and iUPQC Systems for Grid Stability, in IEEE Access, vol. 11, pp. 10258-10269, 2023.
14. C. R. Reddy, P. P. Raj, P. V. V. Satyanarayana, B. N. Reddy, O. C. Sekhar, and B. S. Goud, Improved ZSI-Based DVR for Power Quality Improvement in Grid Connected PV Systems, in Proceedings of the 2022 4th International Conference on Circuits, Control, Communication and Computing (I4C), 2022, pp. 153-157.
15. B. S. Goud, C. N. S. Kalyan, D. Krishna, B. N. Reddy, M. Bajaj, M. F. Ansari, and R. K. Barik, Novel Optimization Techniques and Controllers for Power Quality Improvement, in Proceedings of the 2023 1st International Conference on Circuits, Power and Intelligent Systems (CCPIS), 2023, pp. 1-6.